Provisional chapter

Spatial Atomic Layer Deposition

David Muñoz-Rojas, Viet Huong Nguyen, César Masse de la Huerta, Carmen Jiménez and Daniel Bellet

Additional information is available at the end of the chapter

Abstract

In conventional atomic layer deposition (ALD), precursors are exposed sequentially to a substrate through short pulses while kept physically separated by intermediate purge steps. Spatial ALD (SALD) is a variation of ALD in which precursors are continuously supplied in different locations and kept apart by an inert gas region or zone. Film growth is achieved by exposing the substrate to the locations containing the different precursors. Because the purge step is eliminated, the process becomes faster, being indeed compatible with fast-throughput techniques such as roll-to-roll (R2R), and much more versatile and easier and cheap to scale up. In addition, one of the main assets of SALD is that it can be performed at ambient pressure and even in the open air (i.e., without using any deposition chamber at all), while not compromising the deposition rate. In the present chapter, the fundamentals of SALD and its historical development are presented. Then, a succinct description of the different engineering approaches to SALD developed to date is provided. This is followed by the description of the particular fluid dynamics aspects and the engineering challenges associated with SALD. Finally, some of the applications in which the unique assets of SALD can be exploited are described.

Keywords: chemical vapor deposition, spatial atomic layer deposition (SALD), atmospheric pressure, in-line processing, thin films, transparent conductive materials, fluid dynamics

1. Introduction

The ALD technique was patented in 1977 by Suntola and Antson [1]. It is based on the self-terminating, surface-limited reactions of volatile precursor molecules with a substrate. As

a result, ALD offers unique assets, namely, precise film thickness control to the nanometer, high-quality materials even at low temperature (thanks to the specific highly reactive nature of ALD precursors), and crack-free, compact and conformal film deposition even over high-aspect-ratio features. In this first patent, both the temporal and the spatial approaches were already proposed. In the former, precursors are injected in consecutive pulses separated by purge steps (and thus separated in time) [2–5]. In the later, precursors are supplied in different locations and it is the substrate that moves from one location to another (thus separated in space, see **Figure 1**) [6–9].

In all the enclosures proposed in Suntola's first patent, the reaction takes place inside deposition chambers that operate under vacuum. Curiously enough, although the three first reactors proposed by Suntola were spatial, followed by two temporal reactors (**Figure 2**), ALD has traditionally been developed only based on temporal approaches, both industrially and at the laboratory level, until recently. Some years afterward, in a new patent from 1983, Suntola introduced the idea of using an inert gas flow to separate the different precursors, as an alternative to purging under vacuum [10]. He again applied this principle to both temporal and spatial reactors (**Figure 3**). This was supported by an analytical study of precursor diffusion across the inert gas flow as a function of reactor design and gas flow rate and pulse time. The analysis showed that it was possible to conceive SALD reactors that could operate at ambient pressure without the need of unrealistic inert gas barrier flows, making atmospheric pressure SALD (AP-SALD) possible.

Thus, from the chemical point of view, spatial ALD is equivalent to temporal ALD, and therefore, self-terminating, surface-limited reactions occur. As a consequence, SALD also offers a highly precise growth per cycle, the ability to conformally coat high-aspect-ratio features, and the possibility to deposit high-quality films at lower temperatures than with chemical vapor deposition (CVD). But in addition to retaining the unique assets of ALD, SALD can be up to two orders of magnitude faster. Finally, the possibility to perform SALD at atmospheric pressure (AP-SALD), and even in the open air (without using any deposition chamber at all), makes it cheaper and easier to scale up since complex and expensive vacuum processing is not required.

Although the first patent involving atmospheric-pressure SALD dates from 1983, the first report applying the SALD approach was published only in 2004 [11]. After this initial report,

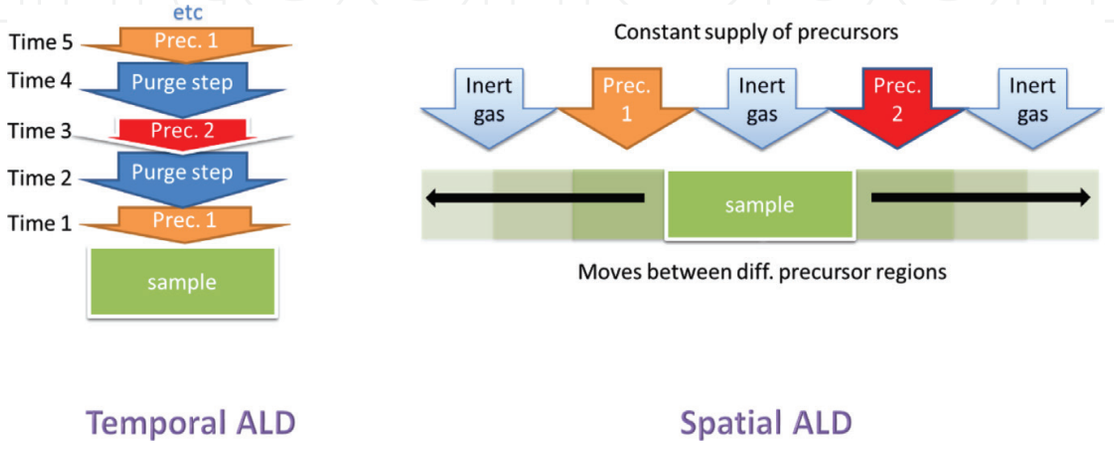

Figure 1. Schema of conventional ALD (left) and of SALD (right).

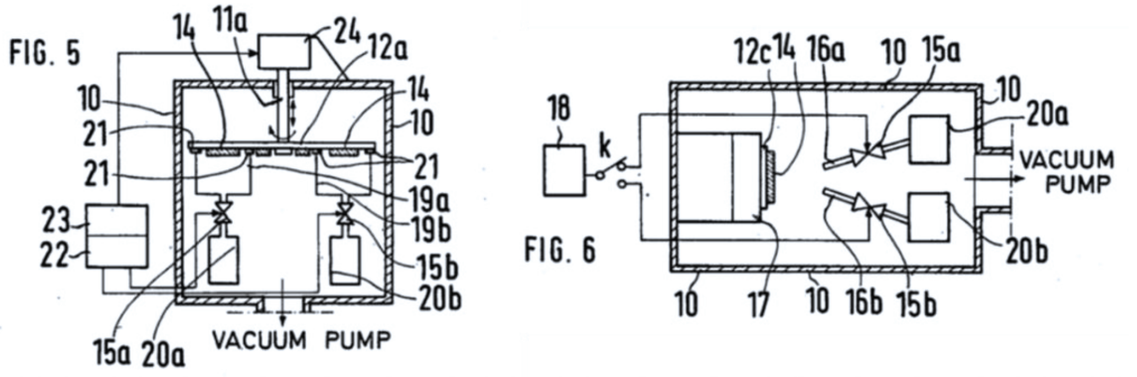

Figure 2. Two of the enclosures proposed by Suntola in his patent from 1977. Left: spatial approach and right: temporal approach.

the SALD field has experienced a significant growth, as shown by the increase in the number of publications dealing with SALD. In addition, many patents have been published since 1983 due to the appropriateness of the AP-SALD approach for application in industry and mass production. The first one by D. Levy (from Kodak) [12] describes a close-proximity, open-air reactor (see Section 2). Rather quickly, SALD has indeed reached industrial commercialization, and several companies are currently developing, fabricating, and/or selling SALD equipment, both for industrial production and for academic research [13].

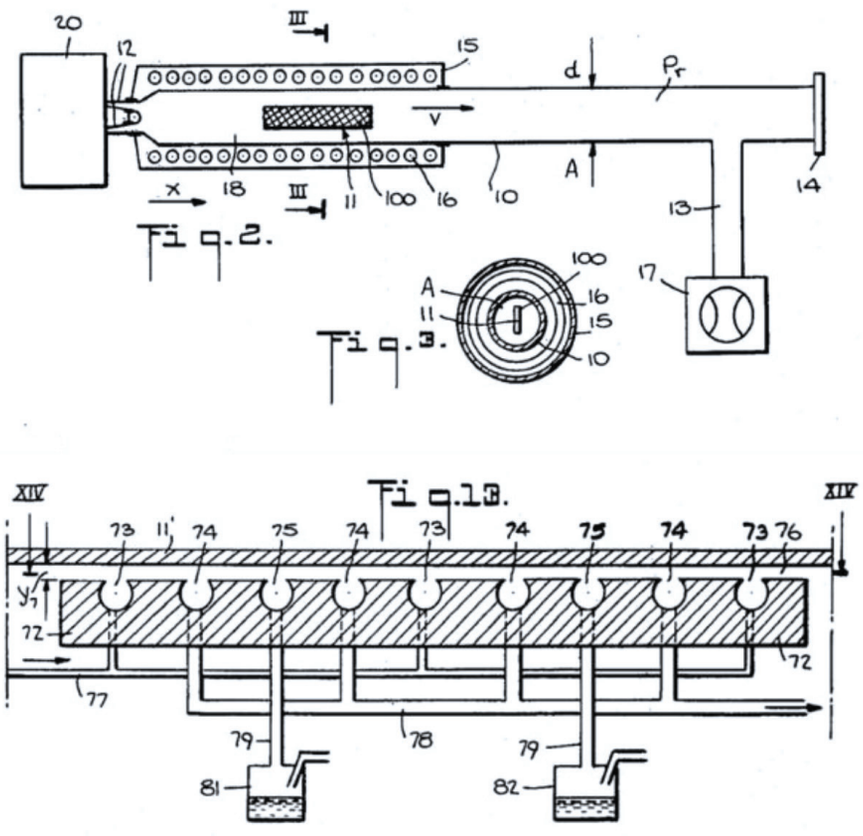

Figure 3. Two of the enclosures proposed by Suntola in his patent from 1983. Top: temporal approach and bottom: spatial approach.

2. Engineering approaches to SALD

The spatial approach has proven to be a very versatile one from the engineering point of view since many reactors have been reported to date. Nonobe et al. reported a spatial horizontal quartz hot-wall type reactor for the growth of HfO_2 films on 10 × 10 mm silicon substrates [11]. $HfCl_4$ (evaporated at 433 K) and O_2 are introduced in opposite sides of the reaction zone using a purified N_2 gas flow. A purified N_2 gas curtain is used to prevent precursors' mixing. Finally, the substrate is oscillated between the different zones by a computer-controlled system. Despite the spatial distribution of the precursors, the precursors are supplied in a temporal fashion, since pulses are delivered to the substrate once it is in place.

Since in most systems, the precursors are continuously fed into the reactor, SALD has also been referred to as continuous ALD. This is the case of the R2R reactor designed by Lotus Applied Technology [14]. In it, a web substrate is moved between reactor zones containing the different precursors, which are separated by a purge zone (**Figure 4**). Differential pressure and pumping are used to prevent precursor migration into the purge zone. Process pressure is generally about 2 mbar. Web speed can reach tens of meters per minute. The reactor has also been configured for plasma-based ALD mode since at high web speeds, it is found that water desorption is not fast enough, thus producing an anomalous growth (see Section 3 for more details).

The ASTRal group from the Lappeenranta University of technology developed a circular reactor for flexible substrates [15]. The design consists of a cylindrical drum to which the flexible substrate is attached. It then rotates inside a reaction chamber containing different precursors and purge zones. The process is equivalent to conventional ALD since the obtained growth per cycle saturates as the precursor flow rate is increased, reaching approximately 1 Å/cycle for the trimethylaluminum (TMA)/water process for the deposition of Al_2O_3 at 100 °C. Prof. Steven M. George's group from the University of Colorado has also developed a modular rotating cylindrical reactor [16]. The design is based on two concentric cylinders. The outer cylinder is fixed and contains several slits that can accept a wide range of modules that attach from the outside (**Figure 5**). The modules can easily move between the various slot positions to perform precursor dosing, purging, or pumping. The inner cylinder rotates with the flexible

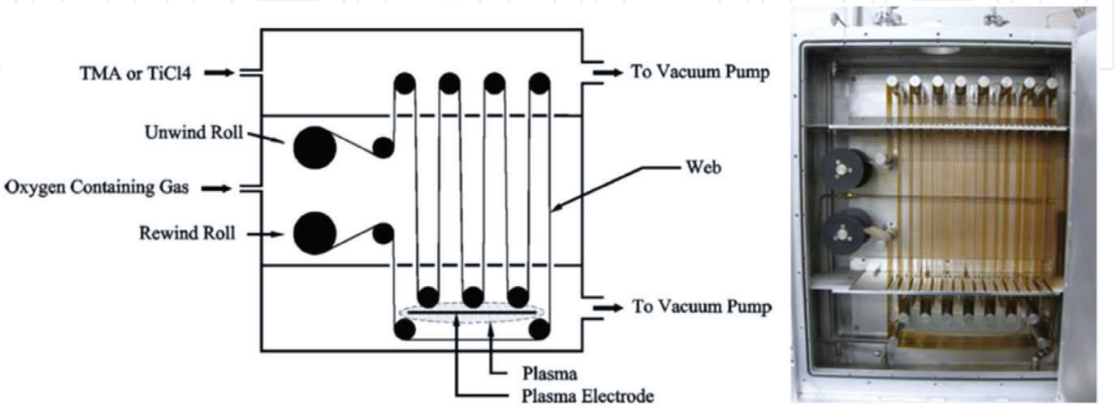

Figure 4. Low-pressure SALD reactor proposed by Lotus Applied Technology. Reproduced from Dickey, E. et al. J. Vac. Sci. Technol. A 30, 021502 (2012), with the permission of the American Vacuum Society.

substrate passing underneath the various spatially separated slits in the outer cylinder. With this reactor, Al_2O_3 films can be grown at a rate of 2 Å/s, for rotation speeds of 175 RPM. Higher deposition rates can even be achieved by adding more modules.

Levy et al. from Kodak designed a very neat approach to AP-SALD in 2008 by [17]. In their approach, an injector manifold head is used to supply the different precursors along parallel channels. The precursors are kept separated by adjacent channels supplying an inert gas flows. Effective precursor separation is attained with practical gas flows (up to thousands of sccm (standard cubic centimeters per minute)) by placing the substrate close to the deposition head (around 50 microns). A relative motion between the head and the substrate replicates the ALD cycles yielding film growth (**Figure 6**). As a result, the system works at atmospheric pressure and even operates in the open air, that is, without using a deposition chamber. In the first model, the injector head was placed on top of the substrate. Later, a different design by Kodak was made in which the head lays at the bottom (the outlets facing upward), with the substrate oscillating on top. Later, other groups, such as the Laboratoire des Matériaux et du Génie Physique (LMGP) in Grenoble (**Figure 6**), have designed similar "close-proximity" SALD setups [18, 19]. In situ monitoring of film thickness has been performed by Yersak et al. taking advantage of the open-air environment offered by such AP-SALD approach. In their work, a reflectometer is placed in series with the injection module in order to monitor film thickness while depositing on a web.to (**Figure 7**) [20].

The close proximity approach, and the effective precursor separation that it provides, has been used in other reactors. TNO (Netherlands Organisation for Applied Scientific Research) has developed a cylindrical reactor consisting of separate zones exposing the precursors one by one to a circular substrate that moves underneath the precursor injector [21]. Between and around the reaction zones, shields of inert gas separate the precursor flows. Under the right operating conditions, these gas shields act as gas bearings, facilitating virtually frictionless movement between reactor and substrate. The group in TNO has also used this type of reactor to do plasma-activated SALD [22, 23]. The same group has also developed an R2R type of reactor based on the close proximity approach similar to the one developed by George's

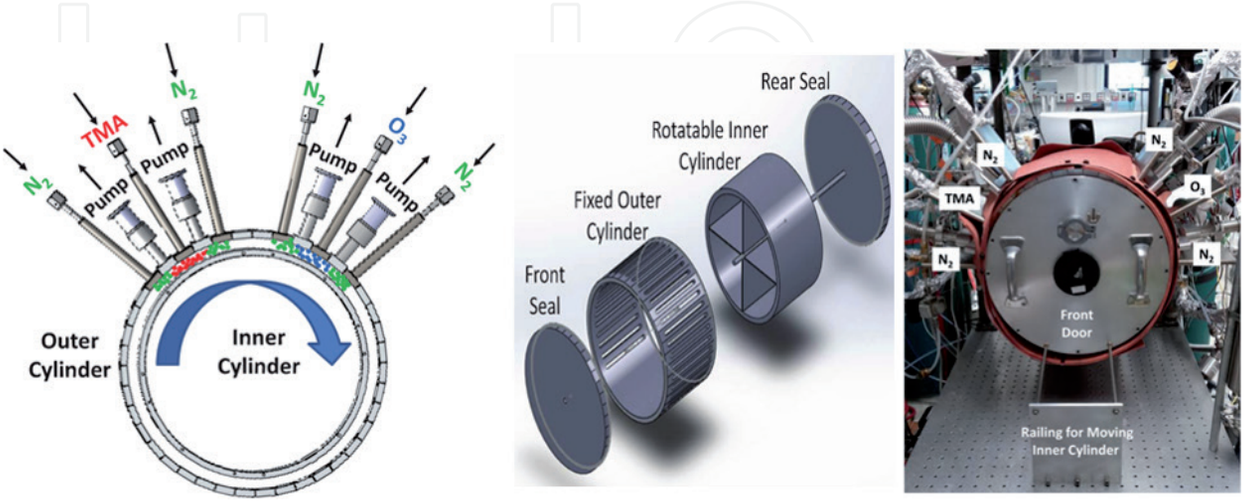

Figure 5. SALD reactor developed at the University of Colorado. Reproduced from Sharma, K. et al., J. Vac. Sci. Technol. A 33, 01A132 (2015), with the permission of the American Vacuum Society.

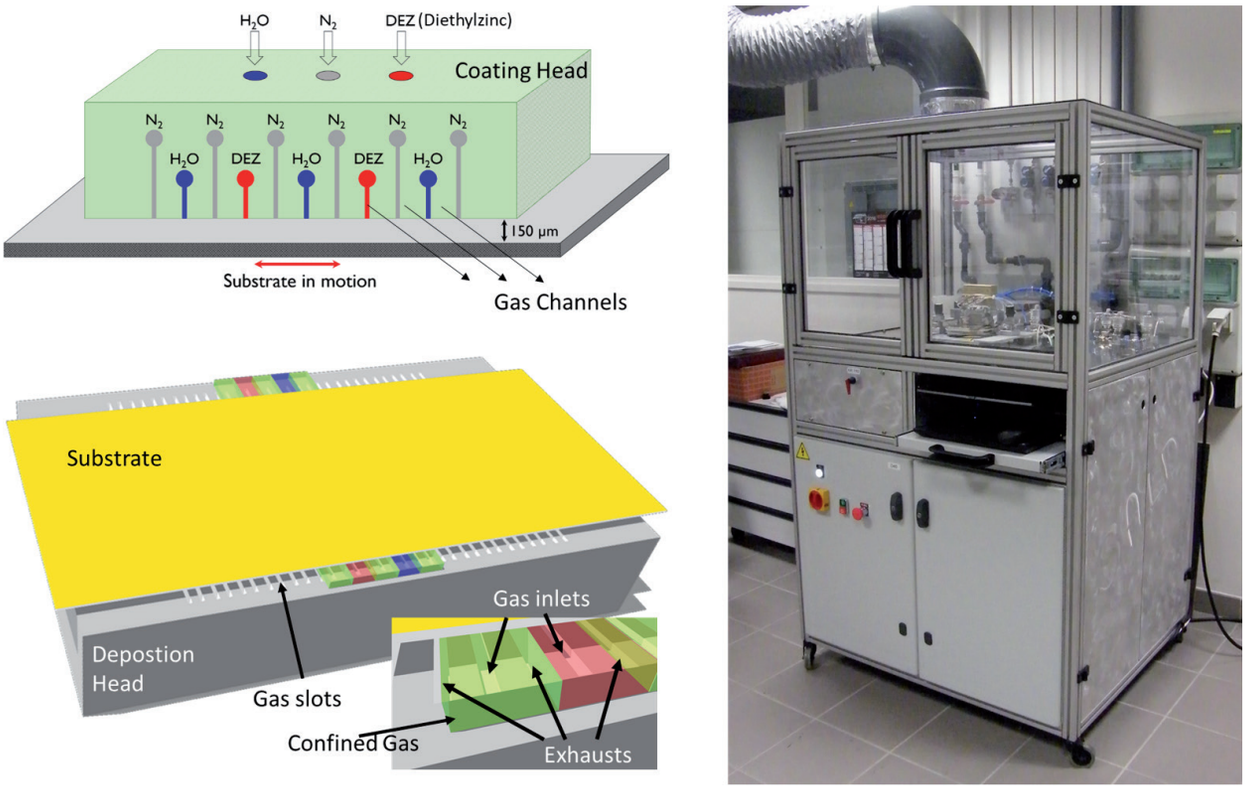

Figure 6. Close-proximity SALD approaches. Left: Schemes of the initial SALD systems reported by Kodak. Right: system developed at the LMGP.

group in Colorado (described above), but in this case, the gas-bearing principle is used (the web floated onto the gas flows coming out of the inner cylinder). There are indeed several patents concerning substrate floatation [24], and this approach has been used for the Solaytec and Levitech commercial systems (see below).

Finally, Ruud van Ommen et al. from the Delft University of Technology have developed a tubular SALD reactor capable of coating nanoparticles thanks to pneumatic transport (**Figure 8**) [25].

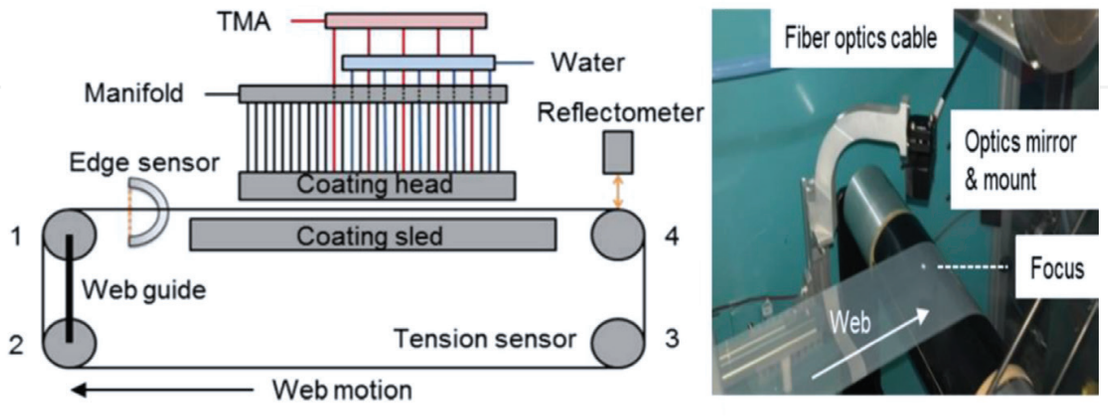

Figure 7. Implementation of in situ film thickness monitoring to an in-line AP-SALD reactor. Reproduced from Yersak, A. S. eta l., J. Vac. Sci. Technol. A 32, 01A130 (2014), with the permission of the American Vacuum Society.

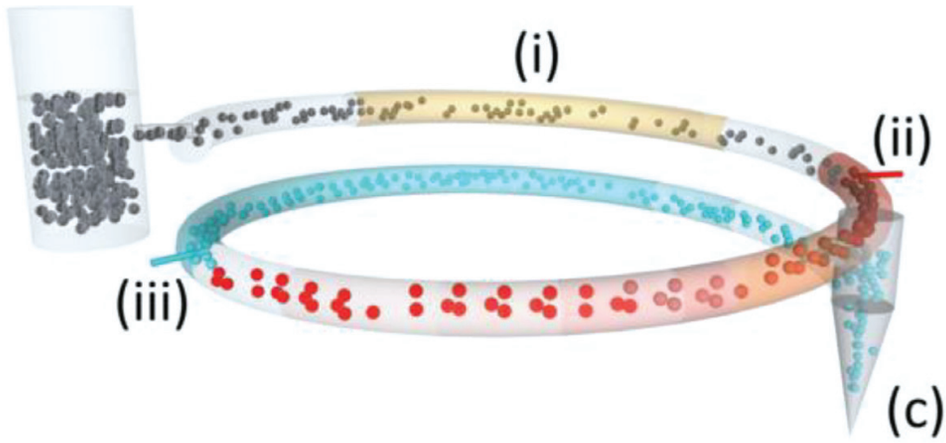

Figure 8. Tubular SALD reactor for coating nanoparticles. Reproduced from van Ommen, J. R. et al., J. Vac. Sci. Technol. A 33, 021513 (2015), with the permission of the American Vacuum Society.

They have developed a 27-m long, 4-mm internal diameter tube reactor, and the substrate nanoparticles (TiO_2 in this case) are fed at about 1 g min^{-1} into the tube from a vessel in which they are suspended in an upward N_2 flow (typically called a fluidized bed). The particles are carried inside the tube at velocities of 5 ms^{-1}. Different sections of the reactor tube contain the different precursor and inert gas purge zones.

The high throughput and scalability of AP-SALD has already been harnessed, and industrial and laboratory equipment is already commercialized. Solaytec (www.solaytec.com), a spin-off from TNO, developed a linear modular close-proximity reactor specially designed to deposit Al_2O_3 passivation layers on silicon solar cells. Levitech (www.levitech.nl) proposes a similar approach. Beneq has as a well-developed, large area R2R industrial coating SALD system (WCS 600), along with the laboratory-scale SALD systems (TFS 200R, R11). A large-scale, large area SALD reactor has recently been presented for the coating of large flat substrates. Applied Materials and Jusung Engineering also propose SALD reactors. SALD is also being used to functionalize commercial products (e.g., plastics) using home-built equipment.

3. SALD fluid dynamics and modeling

From the chemical point of view, SALD is equivalent to ALD and in order to have layer-by-layer surface limited growth, the surface to be coated must be saturated, and any excess precursor that stays physisorbed or laying above the surface should be removed in the purge zone. Since in SALD, the precursors are supplied continuously, efficient separation is a key issue and the reactors must be designed so that the inert flow barriers are effective. As we have seen in the previous section, this has been achieved using various engineering approaches. In order to evaluate the effectiveness of a particular reactor and the effect of the different conditions on the process, modeling is frequently used, as shown below.

The first main advantage of SALD with respect to ALD is that processing can be much faster. The maximum deposition rate that is achievable depends of course on the type of reactor

used, but ultimately, it always depends on the properties of the different precursors and the reaction rate (i.e., reaction kinetics). The time that the substrate is in contact with the precursor flow must be long enough for achieving a complete reaction (i.e., surface saturation). If we take the reaction between TMA and water as an example, the time scale for the TMA half-reaction can be estimated by

$$t_{HR} = \frac{A\chi\, d_{mono}\, \rho_{Al_2O_3}}{c_{gs}\left(M_{Al_2O_3}/M_{TMA}\right) \varnothing_{TMA}} \tag{1}$$

with A being the area available for deposition, χd_{mono} being the self-limiting film thickness, ρ_{Al2O3} the density of the deposited layer, c_{gs} the stoichiometric coefficient, M_{Al2O3} and M_{TMA} are the molar masses of Al_2O_3 and TMA, and $\varnothing_{TMA}$ the precursor mass flow rate. Poodt et al. used this approach to estimate a time scale of a few milliseconds for their reactor [21].

Substrate speed thus needs to be adjusted in order to ensure surface saturation. At the same time, speed may also be limited by the desorption kinetics of precursor molecules physisorbed on the substrate. Water, for example, is known to desorb increasingly slower as temperature diminishes (meaning than in conventional ALD, purging steps become much longer, i.e., 30 s and even minutes), and plasma oxidation is a better choice for low temperatures [14]. The rate of desorption is proportional to the surface concentration, Cs, and on the probability that water molecules desorb. Taking the binding energy of absorbed molecules from the Boltzmann equation, the desorption rate per molecule can be expressed as:

$$R_d = Lexp\left(-\frac{qE}{kT}\right) \tag{2}$$

where L is a constant including the molecular vibrational frequency, E is the molecule binding energy (eV), q is the electronic charge, k is the Boltzmann's constant (JK^{-1}), and T is the temperature (K). The rate of molecules accumulation is then given as:

$$dCs/dt = Is - CsRd \tag{3}$$

where I is the impingement rate of water molecules and s is the sticking coefficient. I can be expressed as

$$I = \frac{P\, N_A}{\sqrt{2\pi MkT}} \tag{4}$$

where N_A is the Avogadro's number, M is the molar mass (kg), and P is the partial pressure of the water vapor. Eq. (3) can thus be solved as

$$C_s = Is\tau\left(1 - \exp\left(-\frac{t}{\tau}\right)\right) \tag{5}$$

where

$$\tau = \frac{1}{R_d} = \frac{1}{L}\exp\left(\frac{qE}{kT}\right) \tag{6}$$

is a time constant. So, the excess of water molecules absorbed on the substrate as a function of time spent in the precursor zone can be approximated as

$$Q_0 = Is\tau\left(1 - exp\left(-1/\tau\right)\right) for\ t > t_m \tag{7}$$

where t_m is the time required for having a monolayer (thus $Q_0 = 0$ for $t < t_m$). From the above discussion, the amount of excess growth (i.e., anomalous CVD growth due to remaining physisorbed water in the substrate) is obtained by combining the water accumulation on the surface while the substrate is in the precursor zone and the desorption taking place in the purging zone:

$$\Delta G = bIs\tau\left(1 - \exp\left(-t/\tau\right)\right)\exp\left(-t/\tau\right) \tag{8}$$

where b is a constant. Thus, temperature, precursor concentration, and speed need to be carefully adjusted in order to ensure minimal excess of absorbed molecules and effective purging. Maydannik et al. used this analytical approach to fit anomalous Al_2O_3 growth obtained experimentally between 100 and 150 °C [26].

The second advantage of SALD is that it can be easily performed at atmospheric pressure and in the open air. For that, the precursors need to be isolated from the atmosphere by the inert gas flow. In its patent from 1983 [10], Suntola developed the equations allowing to estimate the flows that would be required in order to ensure precursor separation and isolation from the ambient. The equations can be applied to temporal ALD reactors and spatial ones, after proper modification taking into account the particular design of each reactor. The equations developed allowed him to predict the viability of atmospheric pressure SALD without the need for unrealistically high inert gas flows.

An important parameter affecting the SALD process is reaction temperature, since it can affect effective precursor separation and the kinetics of the different reactions and processes (such as desorption) taking place. As a consequence, the effective precursor separation and the maximum achievable speed for a particular reactor and reaction can vary for different deposition temperatures. For example, Pan et al. have performed the simulations of a reactor based on the manifold head injector approach [27]. They have used the following set of equations for their simulations:

$$\frac{d\rho}{dt} + \nabla \cdot \left(\rho\vec{V}\right) = 0 \tag{9}$$

$$\frac{d}{dt}d\left(\rho\vec{V}\right) + \nabla \cdot \left(\rho\vec{V}\vec{V}\right) = -\nabla P + \nabla \cdot \tilde{\tau} + \rho\vec{g} + \vec{F} \tag{10}$$

$$\frac{d}{dt}d(\rho\, c_i) + \nabla \cdot \left(\rho\, c_i\vec{V}\right) = -\nabla \cdot \vec{J}_{m,i} + R_i \tag{11}$$

$$\frac{d}{dt}d(\rho E) + \nabla\left[\vec{V}(\rho E + P)\right] = \nabla \cdot \left[k\ \nabla\ T - \sum_i h_i\vec{J}_{h,i} + \left(\tilde{\tau} \cdot \vec{V}\right)\right] \tag{12}$$

where ρ is the density, $\vec{v}$ is the velocity vector, P is the static pressure, $\rho\vec{g}$ and $\vec{F}$ are the gravitational body force and external body forces, respectively, $\tilde{\tau}$ is the stress tensor, ci is the local

molar fraction of species *i*, R_i is the net rate of production of species *i* by chemical reaction, $\vec{J}_{m,i}$ is the mass diffusive flux of mixture species *i*, *k* is the material thermal conductivity, *hi* is the enthalpy of mixture species *i*, and $\vec{J}_{h,i}$ is the energy diffusive flux of mixture species *i*.

The results of the modeling show that temperatures higher than 250 °C accelerate the diffusive mass transport, thus inducing precursor intermixing. On the other hand, high temperature also increases the film deposition rate and results in a higher saturated growth per cycle (GPC) level. The simulation also showed that the chemical deposition process is highly affected by the flow and concentration of precursors. Surface reaction kinetics of the in-line spatial ALD are thus a function of deposition temperature, flow conditions, reactive surface sites, and precursor distributions.

In another example, Deng et al. have presented a numerical model for atmospheric SALD process, based again on an in-line (i.e., manifold injector head) reactor [28]. The effect of inert gas flow rate, carrier gas flow rate, and precursor concentration (i.e., partial pressure or mass fraction) is addressed. The inert gas flow rate obtained from the model agrees well with the experimental values. Simulation results show that the precursor concentration is the determinant factor governing minimal residual time; the optimum precursor usage is inversely proportional to the carrier gas flow rate. Thus, for a constant carrier gas flow, the optimal precursor usage and the precursor mass fraction form a monotonic decreasing relationship. The gap between the gas head and the substrate, regardless of its specific structures in any SALD system, leads to a low Péclet number, thus implying that precursor diffusion plays a more important role than convection.

Finally, due to the relative movement between the substrate and the different gas zones, the possibility of carrying some precursor molecules from one precursor zone to the second precursor zone across the inert gas barrier is not negligible. This precursor entrainment is very much related to the sample speed and to the inert gas flow rate. The movement between a surface and a gas gives rise to a boundary layer at the surface having a thickness inversely proportional to the square root of the relative velocity [15, 26]. The relationship between layer thickness, δ, and substrate speed (Vs) can be expressed as:

$$\delta \sim \sqrt{\frac{1}{V_s}} \tag{13}$$

The dependence of the concentration of precursor in the boundary layer is proportional to δ, which in turn is proportional to the square root of the substrate residence time (residence time being inversely proportional to substrate velocity). Since precursor concentration falls from maximum to 0 once the substrate enters a purge zone, the total quantity of precursor in the boundary layer can be expressed as $G = (1/2)C_s\delta$, where C_s is the concentration at the substrate surface. G diminishes as the substrate progresses in the purge zone. The flux of precursor out of the boundary layer will depend on the concentration gradient:

$$F(t) = -D\frac{dC}{dx} \approx -D\frac{C_s}{V_s} \approx -D\frac{2G}{V_s^2} \tag{14}$$

where D is the diffusion coefficient of the precursor. A similar approach to the one used above to evaluate the excess growth due to excess precursor physisorption can be used here to evaluate anomalous growth rate due to precursor entrainment.

For close-proximity systems, the gap between injector and sample is very important in order to ensure no mixing of the precursors in the gas phase. Nevertheless, for systems for which the gap can be adjusted mechanically, there is also the possibility to perform the deposition in a pseudo-CVD (or spatial CVD, SCVD) mode, that is, allowing a partial mixing of precursors immediately above the substrate. For samples not having complicated or high-aspect-ratio features, not having CVD is not an issue and the obtained films are still dense, uniform, and the thickness obtained is proportional to the number of cycles [29]. In order to control the deposition mode, computational fluid dynamic approaches (CFD) can be used to simulate the process (**Figure 9**). It is also important to consider that the properties and the morphologies of the films obtained using the two different modes (SALD vs. SCVD) are usually different [9].

The possibility of having precursor molecules being entrained from the region where they are being injected to the region where the other precursor is being injected has also to be considered. This is due to the relative movement of the substrate and the injector or precursor zones, and the existence of a boundary layer [15, 19, 20, 30–32]. Again, CFD approaches can be used to predict whether precursor entrainment is to be expected for a set of conditions with a specific SALD system. For example, while many close-proximity systems operate with gap

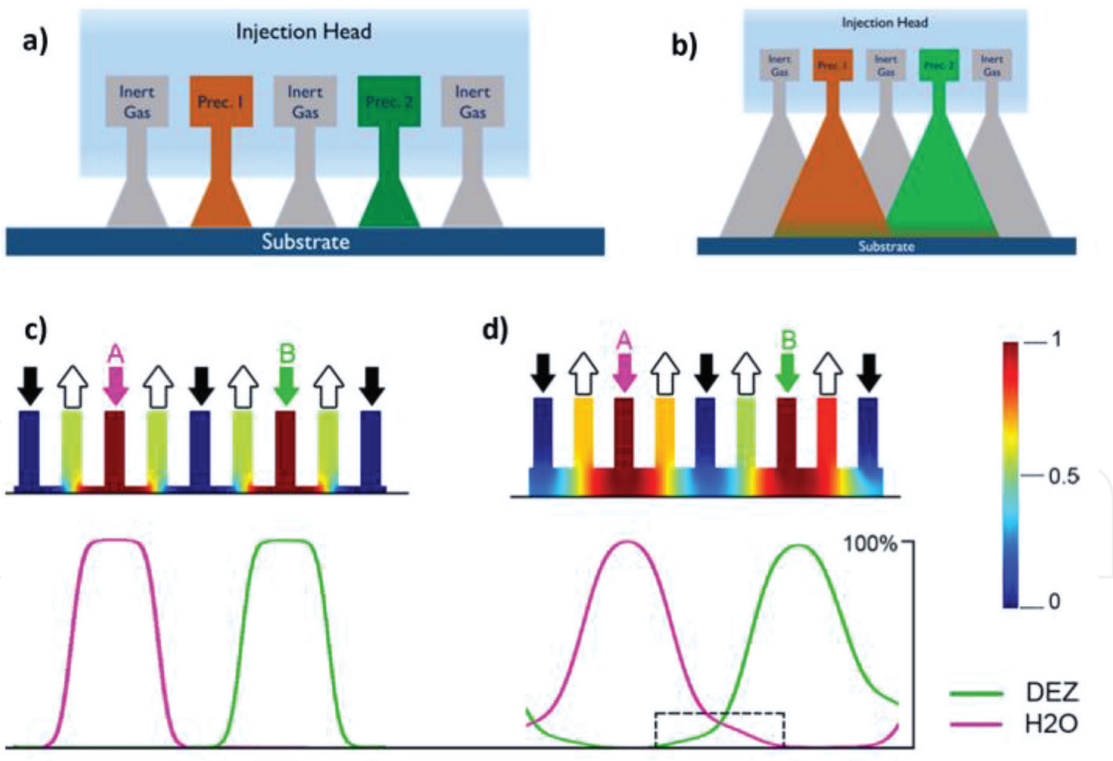

Figure 9. Comparison between SCVD and SALD modes. Scheme of a close-proximity head having two precursor channels and different gaps between head and sample: (a) 150 μm gap, no mixing in the gas phase, (b) 700 μm gap, resulting in precursor mixing above the sample surface, and (c) and (d) show a CFD stationary simulation of the two different modes. A whole representation of the head was used to simulate the behavior of the gases, but only two precursor channels are shown. A cross section of the head with precursor, inert and evacuation channels is shown in which the normalized concentration of the different precursors is given. Below, normalized precursor concentration profiles calculated along the substrate line are shown.

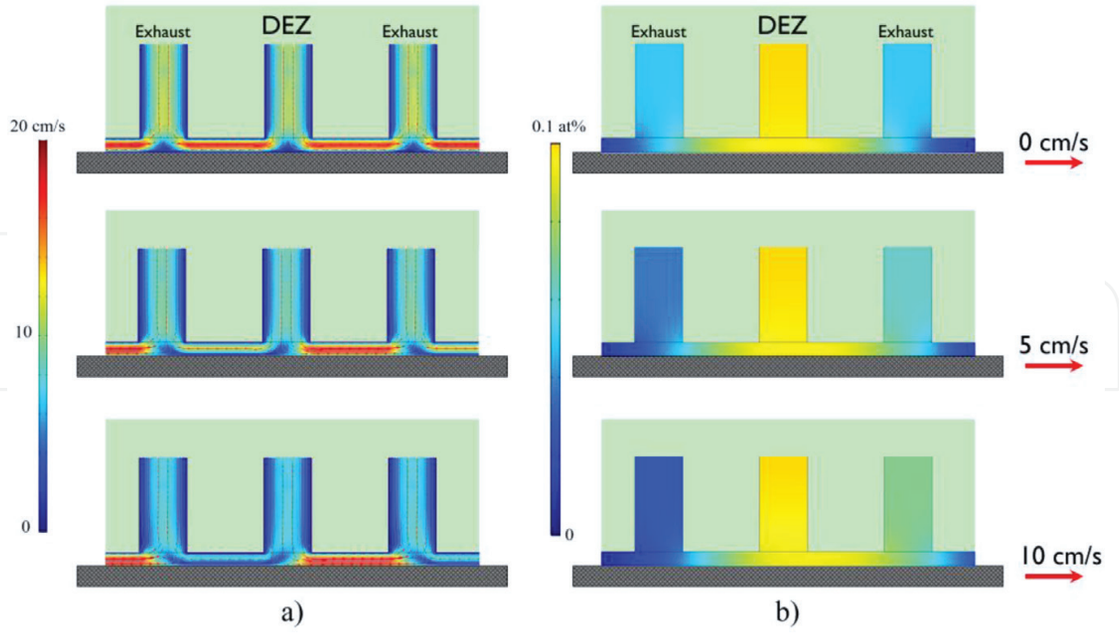

Figure 10. Spatial distribution of (a) precursor velocity and (b) precursor concentration above the substrate for the deposition of ZnO from diethyl zinc (DEZ). Here, only the cross-section views including a DEZ inlet and two exhaust inlets are shown. The blue color corresponds to low velocity/precursor concentration, while red or yellow color corresponds to high velocity/precursor concentration.

sizes in the order of 100 μm, Pan et al. have shown that injector-substrate gaps of as a much as 1.5 mm can be used without having precursor cross-talk [27]. **Figure 10** shows a simulation of the effect of substrate speed in the gas velocity and precursor concentration for the close-proximity SALD system at LMGP [9, 33]. As it can be seen, with the conditions used for the simulation, no precursor entrainment takes place between different precursor regions. The evaluation of precursor entrainment has also been monitored experimentally [30]. Finally, it has recently been demonstrated that atmospheric pressure SALD can be used to coat porous substrates with high throughput as long as high precursor partial pressures and molar flows can be reached [34].

4. Taking advantage of SALD

To date, several materials including intrinsic, doped and mixed oxides, metals and recently organic coatings, have been produced using SALD reactors, as detailed in **Table 1**. The applications range from active and passive components for thin film transistors (TFTs), barriers passivation layers to active components for new-generation solar cells. Some examples are briefly described next.

The first application of SALD, from Kodak, involved the deposition of ZnO and Al_2O_3 layers as components in TFTs [17]. The same group has published different studies on this line, including the use of growth inhibitors for the deposition of patterned films, and thus showing that selected area deposition is also possible with spatial ALD [36, 39, 82, 83]. The group from TNO used their rotary reactor to deposit Al_2O_3 passivation layers for silicon solar cells, and the good

Material		References
Intrinsic metal oxides	HfO_2	[11]
	Al_2O_3	[14–16, 19–21, 26, 31, 35–50]
	ZnO	[18, 36, 39, 45, 46, 51–67]
	SnO_x	[68, 69]
	TiO_2	[14, 18, 70–72]
	Cu_2O	[46, 73, 74]
	Nb_2O_5	[71]
	NiO_x	[91]
	ZrO_2	[92, 93]
	MoO_x	[94]
Doped oxides	ZnO:N	[46, 55, 63, 67]
	Al:ZnO	[36, 56, 75]
	$Zn_{1-x}Mg_xO$	[46, 64, 76]
	In:ZnO	[51, 77]
	ZnO:S	[58]
	$TiO_{2-x}Cl_{2x}$	[78]
Mixed oxides	IGZO	[79]
	CIGS	[80]
Metals	Ag	[23]
	Pt	[25]
Organic materials	Polyamide	[81]

Table 1. Materials deposited by SALD to date.

results prompted the creation of the spinoff company Solaytec (see above) [21]. The same group has dedicated efforts to deposit transparent conductive oxides (TCO) layers and more complex oxides for application in photovoltaic devices [51, 56, 84, 85]. Prof. Driscoll's group was the first one to apply the SALD technique for the deposition of active layers for new-generation solar cells [52, 71–74]. For example, Muñoz-Rojas et al. showed that a 15-nm thick amorphous TiO_2 layer can act as an efficient hole blocking layer in bulk heterojunction solar cells [72]. Thanks to the high quality offered by the SALD technique, an extremely thin (yet crack and pinhole free) layer can be used. And as a result, low deposition temperatures can be used, since the lower conductivity of amorphous TiO_2 is compensated by having a very thin layer. In addition, deposition rates are two orders of magnitude faster than for other low-temperature, atmospheric deposition methods (**Figure 11**). Such high throughput characteristic of SALD is of high relevance for organic-based PV technology. Recently, it has also been shown that SnO_x and ZnO films deposited by SALD can have a beneficial impact on the stability of hybrid perovskite solar cells [62, 69].

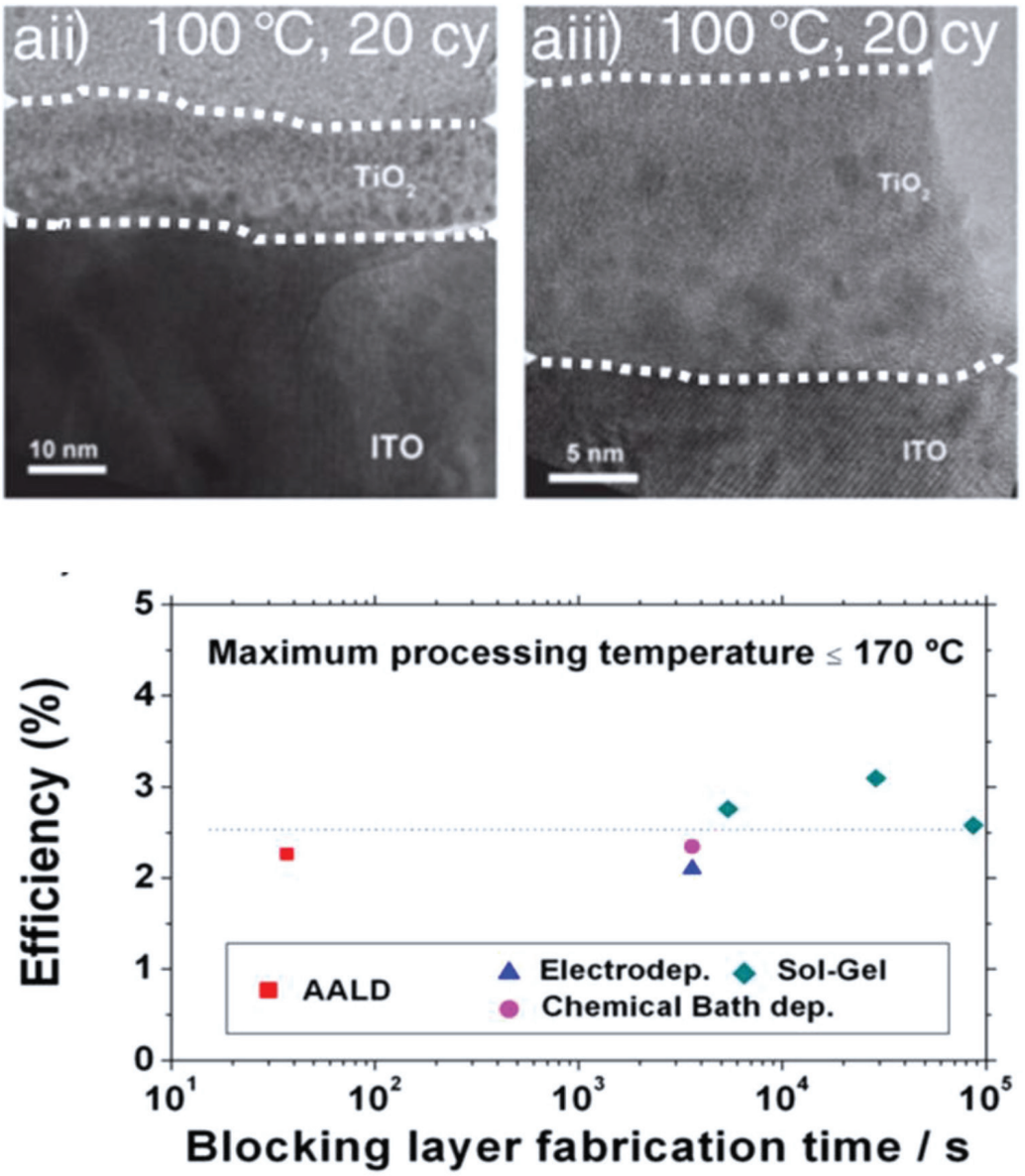

Figure 11. Top: TEM images of TiO_2 amorphous films deposited at 100 °C. Bottom: cell efficiency compared with equivalent cells from the literature in terms of blocking layer fabrication time [72].

SALD has also been used for LEDs, in some cases to deposit active ZnO layers for polymer and hybrid perovskite-based diodes [54, 76], and in another case using Al_2O_3 as permeation barrier for flexible organic LEDs [49]. Other authors have also demonstrated the suitability of SALD for depositing barrier and encapsulation layers both on plastic and paper substrates [14, 31, 40, 48].

K. Sharma et al. used their cylindrical reactor (the University of Colorado, see Section 2) to study the deposition of ZnO on 25 μm thick flexible anodized aluminum oxide (AAO) templates [86]. They used DEZ and ozone as precursors, and the reaction temperature was set at 50 °C. The results show that pores with 100 nm of diameter can be conformally coated for substrate speeds ≤10 RPM. This corresponds to an aspect ratio of 250, and the corresponding residence time is 48 ms. For faster substrate speeds or smaller pores, the films were not

uniform along the pores. Coating of the AAO was used to evaluate the conditions for coating porous substrates. They then used optimized conditions to coat porous Li battery electrodes. The Al_2O_3 SALD coating used was observed to enhance the capacity stability of the electrodes. Other recent studies show the benefits of SALD for the field of energy storage [45, 78].

Chen et al. have developed a system in which two injector heads are combined for the deposition of ZnO/TiO_2 nanolaminates [18]. They show that nanolaminates with the same thickness and overall composition could be turned from crystalline to amorphous by increasing the number of bilayers (i.e., by reducing the thickness of each individual bilayer). Optical transmittance of the laminates increases in the visible range with the number of bilayers. The refractive index of laminates increases with decreasing bilayer thickness, thus demonstrating the possibility for tuning. The conductivity of nanolaminates is higher than for ZnO films due to an increase in carrier density. On the other hand, mobility decreases with respect to intrinsic ZnO layers.

Recent reports from Muñoz-Rojas and coworkers have shown that SALD is an ideal technique to enhance the stability of transparent electrodes based on metallic nanowires (MNWs). In these electrodes, metallic nanowires are deposited by different low-cost, scalable methods, such as spray coating, to obtain a random network. Above a certain areal mass density of the electrode (i.e., amount of nanowires), percolation of the nanowires occurs and the electrode becomes conductive. Yet, since most of the space is empty, the electrode remains transparent. The best electrodes based on AgNWs are comparable and even better than the state-of-the-art indium tin oxide (ITO, the most commonly used transparent conductive oxide) electrodes [87–89]. In addition, electrodes based on MNWs are flexible, which in combination with the soft deposition methods used to fabricate the networks, and make this technology

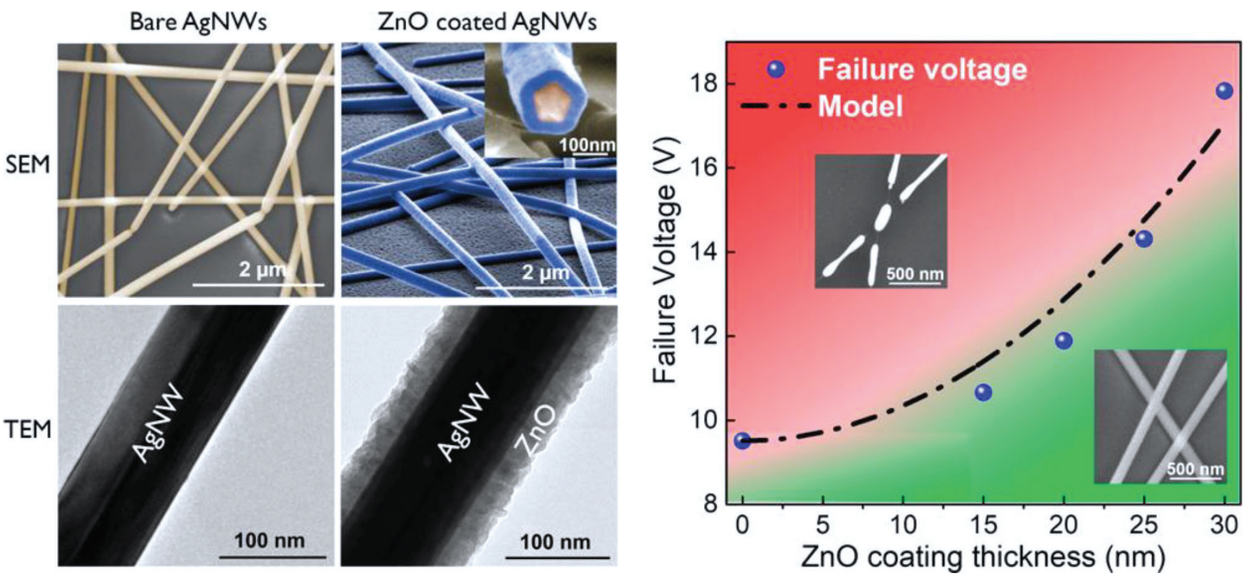

Figure 12. Left: SEM and TEM images of bare and ZnO-coated AgNWs. Right: failure voltage of AgNWs networks versus ZnO coating thickness. The insets correspond to SEM images of a network in which the wires have started spheroidizing due to thermal and electrical instabilities (top), and to a coated network in which the nanowires are intact after being subjected to electrical stress (bottom). The discontinuous line is obtained using a simple model that shows that the enhanced stability of the coated networks is due to hindered Ag atomic diffusion (see reference for details) [61].

compatible with plastic and other soft substrates. Finally, electrodes based on MNWs are more transparent to the infrared part of the spectrum than the transparent conductive oxides (TCO). Despite these advantages, electrodes made of MNWs suffer from thermal, electrical, and chemical instabilities. A solution to increase the stability of the nanowires is to coat them with a thin oxide film, which prevents the diffusion of metal atoms in the wires and the reaction of the same with the atmosphere. ALD is a perfect technique for that since the coatings obtained are dense and crack free. But conventional ALD is usually performed in vacuum, and growth rate is too low. SALD on the other hand can be processed in the open air and offers a high deposition throughput. The close-proximity system at the LMGP has thus been used to coat MNW electrodes. In a first example, ZnO coatings of different thicknesses were deposited on an AgNWs electrode. The oxide coating resulted in a better electrical and thermal stability of the electrodes, and the improvement observed was directly proportional to the thickness of the oxide layer (**Figure 12**) [61]. In another example, Al_2O_3 coatings were used to protect CuNWs electrode. The encapsulation of the wires with the Al_2O_3 layer prevented the oxidation of the wires upon heating in the atmosphere, which allowed the fabrication of stable transparent heaters [44].

5. Conclusions

Although already patented in 1977 at the same time than temporal ALD, spatial ALD has only been developed with the beginning of the twenty-first century. The possibility to perform ALD in much faster deposition rate, at atmospheric pressure and even in the open air has converted SALD in to a technique that is gaining much attention and momentum. SALD has also made the transition from laboratory to industrial scale, and different commercial systems are already available both for laboratory and production scale, while home-made systems are also used. SALD is a very flexible deposition technology that allows a high degree of design freedom, as shown by the increasing number of reactors being developed. Because in SALD, precursors are continuously being injected, efficient separation by the inert gas flow/zone needs to be ensured. The analytical study of fluid dynamics and modeling are thus commonly used during the design of reactors and to evaluate optimum deposition conditions.

Many materials have been already deposited using SALD. Initial works focused on Al_2O_3 and ZnO. Later on, other binary oxides such as Cu_2O, TiO_2, or Nb_2O_5 have been developed, together with the deposition of more complex oxides (including doping and mixes oxides), metals, and even organic films, in which is the first example of spatial molecular layer deposition (SMLD) [90]. The main applications of SALD to date have been for the deposition of components for TFTs, solar cells, and LEDs and for the deposition of barrier and encapsulation layers. SALD has been demonstrated on flexible substrates such as paper or plastic and even on features with high aspect ratios.

The combination of the unique assets of ALD with faster deposition rates and air processing, design flexibility, and easy scalability are expected to make SALD one of the main thin-film deposition techniques in the coming years.

Acknowledgements

David Muñoz-Rojas acknowledges funding through the Marie Curie Actions (FP7/2007-2013, grant agreement no. 631111). DMR also acknowledges funding from the European Union's Horizon 2020 FETOPEN-1-2016-2017 research and innovation programme under grant agreement 801464. The authors thank the Agence Nationale de Recherche (ANR, France) for funding via the projects INDEED (no. ANR-15-CE05-0019) and DESPATCH (no. ANR-16-CE05-0021). This project has received funding from the European Union's Horizon 2020 research and innovation program under grant agreement no. 801464. Viet Huong Nguyen thanks the "ARC Energy Auvergne-Rhône Alpes" for the economic support for Ph.D. grants. César Masse de la Huerta acknowledges and thanks the funding received by CONACYT, Mexico. This work is supported by the French National Research Agency in the framework of the "Investissements d'avenir" program (ANR-15-IDEX-02) through the project Eco-SESA. This project was also financially supported by the "Carnot Énergies du futur" Institute (Aldash Project).

Conflict of interest

The authors declare no conflict of interest.

Author details

David Muñoz-Rojas*, Viet Huong Nguyen, César Masse de la Huerta, Carmen Jiménez and Daniel Bellet

*Address all correspondence to: david.munoz-rojas@grenoble-inp.fr

Université Grenoble Alpes, CNRS, Grenoble INP, LMGP, Grenoble, France

References

[1] Suntola TS, Antson J, Method for Producing Compound Thin Films. US 4,058,430. 1977

[2] George SM. Atomic layer deposition: An overview. Chemical Reviews. 2010;**110**:111-131. DOI: 10.1021/cr900056b

[3] Leskelä M, Ritala M, Nilsen O. Novel materials by atomic layer deposition and molecular layer deposition. MRS Bulletin. 2011;**36**:877-884. DOI: 10.1557/mrs.2011.240

[4] Puurunen RL. Surface chemistry of atomic layer deposition: A case study for the trimethylaluminum/water process. Journal of Applied Physics. 2005;**97**:121301. DOI: 10.1063/1.1940727

[5] Knez M, Nielsch K, Niinistö L. Synthesis and surface engineering of complex nanostructures by atomic layer deposition. Advanced Materials. 2007;**19**:3425-3438. DOI: 10.1002/adma.200700079

[6] Poodt P, Cameron DC, Dickey E, George SM, Kuznetsov V, Parsons GN, et al. Spatial atomic layer deposition: A route towards further industrialization of atomic layer deposition. Journal of Vacuum Science & Technology A—Vacuum Surfaces and Films. 2012;**30**:010802. DOI: 10.1116/1.3670745

[7] Muñoz-Rojas D, MacManus-Driscoll J. Spatial atmospheric atomic layer deposition: A new laboratory and industrial tool for low-cost photovoltaics. Materials Horizons. 2014;**1**: 314-320. DOI: 10.1039/c3mh00136a

[8] Musselman KP, Uzoma CF, Miller MS. Nanomanufacturing: High-throughput, cost-effective deposition of atomic scale thin films via atmospheric pressure spatial atomic layer deposition. Chemistry of Materials. 2016;**28**:8443-8452. DOI: 10.1021/acs.chemmater.6b03077

[9] Muñoz-Rojas D, Nguyen VH, Masse de la Huerta C, Aghazadehchors S, Jiménez C, Bellet D. Spatial Atomic Layer Deposition (SALD), an emerging tool for energy materials. Application to new-generation photovoltaic devices and transparent conductive materials. Comptes Rendus Physique. 2017;**1**:1-10. DOI: 10.1016/j.crhy.2017.09.004

[10] Suntola TS, Pakkala AJ, Lindfors SG. Apparatus for Performing Growth of Compound Thin Films. US 4,389,973. 1983

[11] Nonobe S, Takahashi N, Nakamura T. Preparation of HfO_2 nano-films by atomic layer deposition using $HfCl_4$ and O_2 under atmospheric pressure. Solid State Sciences. 2004;**6**: 1217-1219. DOI: 10.1016/j.solidstatesciences.2004.07.030

[12] Levy DH. Process for Atomic Layer Deposition. US 7,413,982 B2. 2008

[13] Muñoz-Rojas D, Maindron T, Esteve A, Piallat F, Kools J, Decamps M. Speeding up the unique assets of atomic layer deposition. Materials Today Chemistry. 2018

[14] Dickey E, Barrow WA. High rate roll to roll atomic layer deposition, and its application to moisture barriers on polymer films. Journal of Vacuum Science & Technology A—Vacuum Surfaces and Films. 2012;**30**:021502. DOI: 10.1116/1.3678486

[15] Maydannik PS, Kääriäinen TO, Cameron DC. An atomic layer deposition process for moving flexible substrates. Chemical Engineering Journal. 2011;**171**:345-349. DOI: 10.1016/j.cej.2011.03.097

[16] Sharma K, Hall RA, George SM. Spatial atomic layer deposition on flexible substrates using a modular rotating cylinder reactor. Journal of Vacuum Science & Technology A—Vacuum Surfaces and Films. 2015;**33**:01A132. DOI: 10.1116/1.4902086

[17] Levy DH, Freeman D, Nelson SF, Cowdery-Corvan PJ, Irving LM. Stable ZnO thin film transistors by fast open air atomic layer deposition. Applied Physics Letters. 2008;**92**:192101. DOI: 10.1063/1.2924768

[18] Chen R, Lin J-L, He W-J, Duan C-L, Peng Q, Wang X-L, et al. Spatial atomic layer deposition of ZnO/TiO_2 nanolaminates. Journal of Vacuum Science & Technology A—Vacuum Surfaces and Films. 2016;**34**:051502. DOI: 10.1116/1.4955289

[19] Ryan Fitzpatrick P, Gibbs ZM, George SM. Evaluating operating conditions for continuous atmospheric atomic layer deposition using a multiple slit gas source head. Journal of Vacuum Science & Technology A—Vacuum Surfaces and Films. 2012;**30**:01A136. DOI: 10.1116/1.3664765

[20] Yersak AS, Lee YC, Spencer JA, Groner MD. Atmospheric pressure spatial atomic layer deposition web coating with in situ monitoring of film thickness. Journal of Vacuum Science & Technology A—Vacuum Surfaces and Films. 2014;**32**:01A130. DOI: 10.1116/1.4850176

[21] Poodt P, Lankhorst A, Roozeboom F, Spee K, Maas D, Vermeer A. High-speed spatial atomic-layer deposition of aluminum oxide layers for solar cell passivation. Advanced Materials. 2010;**22**:3564-3567. DOI: 10.1002/adma.201000766

[22] Poodt P, Kniknie B, Branca A, Winands H, Roozeboom F. Patterned deposition by plasma enhanced spatial atomic layer deposition. Physica Status Solidi (RRL)—Rapid Research Letters. 2011;**5**:165-167. DOI: 10.1002/pssr.201004542

[23] van den Bruele FJ, Smets M, Illiberi A, Creyghton Y, Buskens P, Roozeboom F, et al. Atmospheric pressure plasma enhanced spatial ALD of silver. Journal of Vacuum Science & Technology A—Vacuum Surfaces and Films. 2015;**33**:01A131. DOI: 10.1116/1.4902561

[24] Levy DH. Deposition System and Method Using a Delivery Head Separated Froma Substrate by Gas Pressure. US 2009/0130858, US 2010/0311130 Al. 2009

[25] van Ommen JR, Kooijman D, de Niet M, Talebi M, Goulas A. Continuous production of nanostructured particles using spatial atomic layer deposition. Journal of Vacuum Science & Technology A—Vacuum Surfaces and Films. 2015;**33**:021513. DOI: 10.1116/1.4905725

[26] Maydannik PS, Kaariainen TO, Cameron DC. Continuous atomic layer deposition: Explanation for anomalous growth rate effects. Journal of Vacuum Science & Technology A—Vacuum Surfaces and Films. 2012;**30**:01A122. DOI: 10.1116/1.3662861

[27] Pan D, Jen T-C, Yuan C. Effects of gap size, temperature and pumping pressure on the fluid dynamics and chemical kinetics of in-line spatial atomic layer deposition of Al_2O_3. International Journal of Heat and Mass Transfer. 2016;**96**:189-198. DOI: 10.1016/j.ijheatmasstransfer.2016.01.034

[28] Deng Z, He W, Duan C, Chen R, Shan B. Mechanistic modeling study on process optimization and precursor utilization with atmospheric spatial atomic layer deposition. Journal of Vacuum Science & Technology A—Vacuum Surfaces and Films. 2016;**34**:01A108. DOI: 10.1116/1.4932564

[29] Hoye RLZ, Muñoz-Rojas D, Musselman KP, Vaynzof Y, MacManus-Driscoll JL. Synthesis and modeling of uniform complex metal oxides by close-proximity atmospheric pressure chemical vapor deposition. ACS Applied Materials & Interfaces. 2015;**7**:10684-10694. DOI: 10.1021/am5073589

[30] Maydannik PS, Kääriäinen TO, Lahtinen K, Cameron DC, Söderlund M, Soininen P, et al. Roll-to-roll atomic layer deposition process for flexible electronics encapsulation applications. Journal of Vacuum Science and Technology A. 2014;**32**:51603. DOI: 10.1116/1.4893428

[31] Maydannik PS, Plyushch A, Sillanpää M, Cameron DC, Cameron DC. Spatial atomic layer deposition: Performance of low temperature H_2O and O_3 oxidant chemistry for flexible electronics encapsulation. Journal of Vacuum Science and Technology A. 2015;**33**:031603. DOI: 10.1116/1.4914079

[32] Levy DH, Nelson SF, Freeman D. Oxide electronics by spatial atomic layer deposition. Journal of Display Technology. 2009;**5**:484-494. Available from: http://jdt.osa.org/abstract.cfm?URI=jdt-5-12-484 [Accessed: Jun 27, 2012]

[33] Nguyen VH, Resende J, Jiménez C, Deschanvres J, Carroy P, Muñoz D, et al. Deposition of ZnO based thin films by atmospheric pressure spatial atomic layer deposition for application in solar cells. Journal of Renewable and Sustainable Energy. 2017;**9**:021203. DOI: 10.1063/1.4979822

[34] Poodt P, Mameli A, Schulpen J, Roozeboom WMMEK, Roozeboom F. Effect of reactor pressure on the conformal coating inside porous substrates by atomic layer deposition. Journal of Vacuum Science and Technology A. 2017:021502. DOI: 10.1116/1.4973350

[35] Suh S, Park S, Lim H, Choi Y-J, Seong Hwang C, Joon Kim H, et al. Investigation on spatially separated atomic layer deposition by gas flow simulation and depositing Al_2O_3 films. Journal of Vacuum Science & Technology A—Vacuum Surfaces and Films. 2012;**30**:051504. DOI: 10.1116/1.4737123

[36] Ellinger CR, Nelson SF. Selective area spatial atomic layer deposition of ZnO, Al_2O_3, and aluminum-doped ZnO using poly(vinyl pyrrolidone). Chemistry of Materials. 2014;**26**: 1514-1522. DOI: 10.1021/cm402464z

[37] Ali K, Choi K-H, Muhammad NM. Roll-to-roll atmospheric atomic layer deposition of Al_2O_3 thin films on PET substrates. Chemical Vapor Deposition. 2014;**20**:1-8. DOI: 10.1002/cvde.201407126

[38] Poodt P, Knaapen R, Illiberi A, Roozeboom F, van Asten A. Low temperature and roll-to-roll spatial atomic layer deposition for flexible electronics. Journal of Vacuum Science & Technology A—Vacuum Surfaces and Films. 2012;**30**:01A142. DOI: 10.1116/1.3667113

[39] Levy DH, Ellinger CR, Nelson SF. Metal-oxide thin-film transistors patterned by printing. Applied Physics Letters. 2013;**103**:043505. DOI: 10.1063/1.4816322

[40] Lahtinen K, Maydannik P, Johansson P, Kääriäinen T, Cameron DC, Kuusipalo J. Utilisation of continuous atomic layer deposition process for barrier enhancement of extrusion-coated paper. Surface and Coatings Technology. 2011;**205**:3916-3922. DOI: 10.1016/j.surfcoat.2011.02.009

[41] Poodt P, van Lieshout J, Illiberi A, Knaapen R, Roozeboom F, van Asten A. On the kinetics of spatial atomic layer deposition. Journal of Vacuum Science & Technology A—Vacuum Surfaces and Films. 2013;**31**:01A108. DOI: 10.1116/1.4756692

[42] Poodt P, Illiberi A, Roozeboom F. The kinetics of low-temperature spatial atomic layer deposition of aluminum oxide. Thin Solid Films. 2013;**532**:22-25. DOI: 10.1016/j.tsf.2012.10.109

[43] Mousa MBM, Ovental JS, Brozena AH, Oldham CJ, Parsons GN. Modeling and experimental demonstration of high-throughput flow-through spatial atomic layer deposition of Al_2O_3 coatings on textiles at atmospheric pressure. Journal of Vacuum Science and Technology A. 2018;**36**:031517. DOI: 10.1116/1.5022077

[44] Celle C, Cabos A, Fontecave T, Laguitton B, Benayad A, Guettaz L, et al. Oxidation of copper nanowire based transparent electrodes in ambient conditions and their stabilization by encapsulation: Application to transparent film heaters. Nanotechnology. 2018;**29**:085701

[45] Yersak AS, Sharma K, Wallas JM, Dameron AA, Li X, Yang Y, et al. Spatial atomic layer deposition for coating flexible porous Li-ion battery electrodes Spatial atomic layer deposition for coating flexible porous Li-ion battery electrodes. Journal of Vacuum Science and Technology A. 2018;**36**:01A123. DOI: 10.1116/1.5006670

[46] Musselman KP, Muñoz-Rojas D, Hoye RLZ, Sun H, Sahonta S-L, Croft E, et al. Rapid open-air deposition of uniform, nanoscale, functional coatings on nanorod arrays. Nanoscale Horizons. 2017;**2**:110-117. DOI: 10.1039/C6NH00197A

[47] Franke S, Baumkötter M, Monka C, Raabe S, Caspary R, Johannes H-H, et al. Alumina films as gas barrier layers grown by spatial atomic layer deposition with trimethylaluminum and different oxygen sources. Journal of Vacuum Science & Technology A—Vacuum Surfaces and Films. 2017;**35**:01B117. DOI: 10.1116/1.4971173

[48] Ali K, Ali J, Mehdi SM, Choi K-H, An YJ. Rapid fabrication of Al2O3 encapsulations for organic electronic devices. Applied Surface Science. 2015;**353**:1186-1194. DOI: 10.1016/j.apsusc.2015.07.032

[49] Choi H, Shin S, Jeon H, Choi Y, Kim J, Kim S, et al. Fast spatial atomic layer deposition of Al_2O_3 at low temperature (<100 °C) as a gas permeation barrier for flexible organic light-emitting diode displays. Journal of Vacuum Science & Technology A—Vacuum Surfaces and Films. 2016;**34**:01A121. DOI: 10.1116/1.4934752

[50] Ali K, Choi K-H. Low-temperature roll-to-roll atmospheric atomic layer deposition of Al_2O_3 thin films. Langmuir. 2014;**30**:14195-14203. DOI: 10.1021/la503406v

[51] Illiberi A, Scherpenborg R, Roozeboom F, Poodt P. Atmospheric spatial atomic layer deposition of In-doped ZnO. ECS Journal of Solid State Science and Technology. 2014;**3**:P111-P114. DOI: 10.1149/2.002405jss

[52] Hoye RLZ, Muñoz-Rojas D, Iza DC, Musselman KP, MacManus-Driscoll JL. High performance inverted bulk heterojunction solar cells by incorporation of dense, thin ZnO layers made using atmospheric atomic layer deposition. Solar Energy Materials & Solar Cells. 2013;**116**:197-202. DOI: 10.1016/j.solmat.2013.04.020

[53] Illiberi A, Scherpenborg R, Theelen M, Poodt P, Roozeboom F. On the environmental stability of ZnO thin films by spatial atomic layer deposition. Journal of Vacuum Science & Technology A—Vacuum Surfaces and Films. 2013;**31**:061504. DOI: 10.1116/1.4816354

[54] Hoye RLZ, Chua MR, Musselman KP, Li G, Lai M-L, Tan Z-K, et al. Enhanced performance in fluorene-free organometal halide perovskite light-emitting diodes using tunable, low electron affinity oxide electron injectors. Advanced Materials. 2015;**20**: 1414-1419. DOI: 10.1002/adma.201405044

[55] Ehrler B, Musselman KP, Böhm ML, Morgenstern FSF, Vaynzof Y, Walker BJ, et al. Preventing interfacial recombination in colloidal quantum dot solar cells by doping the metal oxide. ACS Nano. 2013;**7**:4210-4220. DOI: 10.1021/nn400656n

[56] Illiberi A, Scherpenborg R, Wu Y, Roozeboom F, Poodt P. Spatial atmospheric atomic layer deposition of $Al_xZn_{1-x}O$. ACS Applied Materials & Interfaces. 2013;**5**:13124-13128. DOI: 10.1021/am404137e

[57] Illiberi A, Roozeboom F, Poodt P. Spatial atomic layer deposition of zinc oxide thin films. ACS Applied Materials & Interfaces. 2012;**4**:268-272. DOI: 10.1021/am2013097

[58] Frijters CH, Poodt P, Illiberi A. Atmospheric spatial atomic layer deposition of Zn(O,S) buffer layer for $Cu(In,Ga)Se_2$ solar cells. Solar Energy Materials & Solar Cells. 2016;**155**:356-361. DOI: 10.1016/j.solmat.2016.06.016

[59] Nelson SF, Levy DH, Tutt LW, Burberry M. Cycle time effects on growth and transistor characteristics of spatial atomic layer deposition of zinc oxide. Journal of Vacuum Science & Technology A—Vacuum Surfaces and Films. 2012;**30**:01A154. DOI: 10.1116/1.3670878

[60] Nguyen VH, Gottlieb U, Valla A, Muñoz D, Bellet D, Muñoz-Rojas D. Electron tunneling through grain boundaries in transparent conductive oxides and implications for electrical conductivity: The case of ZnO:Al thin films. Materials Horizons. 2018;**5**:715-726. DOI: 10.1039/C8MH00402A

[61] Khan A, Nguyen VH, Muñoz-Rojas D, Aghazadehchors S, Jiménez C, Nguyen ND, et al. Stability enhancement of silver nanowire networks with conformal ZnO coatings deposited by atmospheric pressure spatial atomic layer deposition. ACS Applied Materials & Interfaces. 2018;**10**:19208-19217. DOI: 10.1021/acsami.8b03079

[62] Najafi M, Zardetto V, Zhang D, Koushik D, Dorenkampe M, Creatore M, et al. Highly efficient semitransparent p-i-n planar perovskite solar cells by atmospheric pressure spatial atomic layer deposited ZnO. Solar RRL. 2018;**2**:1800147. DOI: 10.1002/solr.201800147

[63] Dunlop L, Kursumovic A, MacManus-Driscoll JL. Reproducible growth of p-type ZnO:N using a modified atomic layer deposition process combined with dark annealing. Applied Physics Letters. 2008;**93**:172111. DOI: 10.1063/1.3000604

[64] Hoye RLZ, Ehrler B, Böhm ML, Muñoz-Rojas D, Altamimi RM, Alyamani AY, et al. Improved open-circuit voltage in ZnO-PbSe quantum dot solar cells by understanding and reducing losses arising from the ZnO conduction band tail. Advanced Energy Materials. 2014;**4**:1301544. DOI: 10.1002/aenm.201301544

[65] Nandakumar N, Dielissen B, Garcia-Alonso D, Liu Z, Gortzen R, Kessels WMME, et al. Resistive intrinsic ZnO films deposited by ultrafast spatial ALD for PV applications. IEEE Journal of Photovoltaics. 2015;**5**:1462-1469. DOI: 10.1109/JPHOTOV.2015.2438644

[66] Hoye RLZ, Muñoz-Rojas D, Nelson SF, Illiberi A, Poodt P, Roozeboom F, et al. Research update: Atmospheric pressure spatial atomic layer deposition of ZnO thin films: Reactors, doping, and devices. APL Materials. 2015;**3**:040701. DOI: 10.1063/1.4916525

[67] Musselman KP, Albert-Seifried S, Hoye RLZ, Sadhanala A, Muñoz-Rojas D, MacManus-Driscoll JL, et al. Improved exciton dissociation at semiconducting polymer:ZnO donor: acceptor interfaces via nitrogen doping of ZnO. Advanced Functional Materials. 2014;**24**: 3562-3570 DOI: 10.1002/adfm.201303994

[68] Hoffmann L, Theirich D, Schlamm D, Hasselmann T, Pack S, Brinkmann KO, et al. Atmospheric pressure plasma enhanced spatial atomic layer deposition of SnOx as conductive gas diffusion barrier. Journal of Vacuum Science and Technology A. 2018;**36**:01A112. DOI: 10.1116/1.5006781

[69] Hoffmann L, Brinkmann KO, Malerczyk J, Rogalla D, Becker T, Theirich D, et al. Spatial atmospheric pressure atomic layer deposition of tin oxide as an impermeable Electron extraction layer for perovskite solar cells with enhanced thermal stability. ACS Applied Materials & Interfaces. 2018;**10**:6006-6013. DOI: 10.1021/acsami.7b17701

[70] Aghaee M, Maydannik PS, Johansson P, Kuusipalo J, Creatore M, Homola T, et al. Low temperature temporal and spatial atomic layer deposition of TiO_2 films. Journal of Vacuum Science & Technology A—Vacuum Surfaces and Films. 2015;**33**:041512. DOI: 10.1116/1.4922588

[71] Armstrong CL, Price MB, Muñoz-Rojas D, Davis NJKL, Abdi-Jalebi M, Friend RH, et al. Influence of an inorganic interlayer on exciton separation in hybrid solar cells. ACS Nano. 2015;**9**:11863-11871. DOI: 10.1021/acsnano.5b05934

[72] Muñoz-Rojas D, Sun H, Iza DC, Weickert J, Chen L, Wang H, et al. High-speed atmospheric atomic layer deposition of ultra thin amorphous TiO_2 blocking layers at 100 °C for inverted bulk heterojunction solar cells. Progress in Photovoltaics: Research and Applications. 2013;**21**:393-400. DOI: 10.1002/pip.2380

[73] Marin AT, Muñoz-Rojas D, Iza DC, Gershon T, Musselman KP, MacManus-Driscoll JL. Novel atmospheric growth technique to improve both light absorption and charge collection in ZnO/Cu_2O thin film solar cells. Advanced Functional Materials. 2013;**23**:3413-3419. DOI: 10.1002/adfm.201203243

[74] Muñoz-Rojas D, Jordan M, Yeoh C, Marin AT, Kursumovic A, Dunlop L, et al. Growth of 5 $cm^2\ V^{-1}\ s^{-1}$ mobility, p-type Copper(I)oxide (Cu_2O) films by fast atmospheric atomic layer deposition (AALD) at 225 °C and below. AIP Advances. 2012;**2**:042179. DOI: 10.1063/1.4771681

[75] Fullager DB, Boreman GD, Ellinger CD, Hofmann T. Broadband optical properties of aluminium zinc oxide thin films prepared by spatial atomic layer deposition. Thin Solid Films. 2018;**653**:267-273. DOI: 10.1016/j.tsf.2018.03.047

[76] Hoye RLZ, Musselman KP, Chua MR, Sadhanala A, Raninga RD, Friend RH, et al. Bright and efficient blue polymer light emitting. Journal of Materials Chemistry C. 2015;**3**: 9327-9336. DOI: 10.1039/C5TC01581B

[77] Illiberi A, Frijters C, Ruth M, Bremaud D, Poodt P, Roozeboom F, et al. Atmospheric spatial atomic layer deposition of ZnOS buffer layers for flexible Cu(In,Ga)Se_2 solar cells. Journal of Vacuum Science and Technology A. 2018;**36**:051511. DOI: 10.1116/1.5040457

[78] Moitzheim S, Balder JE, Poodt P, Unnikrishnan S, De Gendt S, Vereecken PM. Chlorine doping of amorphous TiO_2 for increased capacity and faster Li^+-ion storage. Chemistry of Materials. 2017;**29**:10007-10018. DOI: 10.1021/acs.chemmater.7b03478

[79] Illiberi A, Cobb B, Sharma A, Grehl T, Brongersma H, Roozeboom F, et al. Spatial atmospheric atomic layer deposition of $In_xGa_yZn_zO$ for thin films transistors. ACS Applied Materials & Interfaces. 2015;**7**:3671-3675. DOI: 10.1021/am508071y

[80] Illiberi A, Grob F, Frijters C, Poodt P, Ramachandra R, Winands H, et al. High rate (~7 nm/s), atmospheric pressure deposition of ZnO front electrode for Cu(In,Ga)Se_2 thin-film solar cells with efficiency beyond 15%. Progress in Photovoltaics: Research and Applications. 2013;**21**:1559-1566. DOI: 10.1002/pip.2423

[81] Higgs DJ, Dumont JW, Sharma K, George SM. Spatial molecular layer deposition of polyamide thin films on flexible polymer substrates using a rotating cylinder reactor. Journal of Vacuum Science & Technology A—Vacuum Surfaces and Films. 2018;**36**:01A117

[82] Ellinger CR, Nelson SF. Design freedom in multilayer thin-film devices. ACS Applied Materials & Interfaces. 2015;**7**:4675-4684. DOI: 10.1021/am508088p

[83] Nelson SF, Ellinger CR, Levy DH. Improving yield and performance in ZnO thin-film transistors made using selective area deposition. ACS Applied Materials & Interfaces. 2015;**7**:2754-2759. DOI: 10.1021/am5077638

[84] Illiberi A, Poodt P, Bolt P-J, Roozeboom F. Recent advances in atmospheric vapor-phase deposition of transparent and conductive zinc oxide. Chemical Vapor Deposition. 2014; **20**:234-242. DOI: 10.1002/cvde.201400056

[85] Illiberi A, Scherpenborg R, Poodt P, Roozeboom F. (Invited) spatial atomic layer deposition of transparent conductive oxides. ECS Transactions. 2013;**58**:105-110. DOI: 10.1149/05810.0105ecst

[86] Sharma K, Routkevitch D, Varaksa N, George SM. Spatial atomic layer deposition on flexible porous substrates: ZnO on anodic aluminum oxide films and Al_2O_3 on Li ion battery electrodes. Journal of Vacuum Science & Technology A—Vacuum Surfaces and Films. 2016;**34**:01A146. DOI: 10.1116/1.4937728

[87] Bellet D, Lagrange M, Sannicolo T, Aghazadehchors S, Nguyen VH, Langley DP, et al. Transparent electrodes based on silver nanowire networks: From physical considerations towards device integration. Materials (Basel). 2017;**10**:570. DOI: 10.3390/ma10060570

[88] Langley D, Giusti G, Mayousse C, Celle C, Bellet D, Simonato J-P. Flexible transparent conductive materials based on silver nanowire networks: A review. Nanotechnology. 2013;**24**:452001. DOI: 10.1088/0957-4484/24/45/452001

[89] Sannicolo T, Lagrange M, Cabos A, Celle C, Simonato J, Bellet D. Metallic nanowire-based transparent electrodes for next generation flexible devices : A review. Small. 2016;**12**:6052-6075. DOI: 10.1002/smll.201602581

[90] Gregorczyk K, Knez M. Progress in materials science hybrid nanomaterials through molecular and atomic layer deposition: Top down, bottom up , and in-between approaches to new materials. Progress in Materials Science. 2016;**75**:1-37. DOI: 10.1016/j.pmatsci.2015.06.004

[91] Zhao B, Lee LC, Yang L, Pearson AJ, Lu H, She X, et al. In-situ atmospheric deposition of ultra-smooth nickel oxide for efficient perovskite solar cells. ACS Applied Materials & Interfaces. 2018. DOI: 10.1021/acsami.8b15503

[92] Creyghton Y, Illiberi A, Mione A, Boekel W. van, Debernardi N, Seitz M, et al. Plasma-enhanced atmospheric-pressure spatial ALD of Al_2 O_3 and ZrO_2Y. Creyghton. ECS Transation. 2016;**75**:11-19

[93] Mione MA, Katsouras I, Creyghton Y, van Boekel W, Maas J, Gelinck G, et al. Atmospheric pressure plasma enhanced spatial ALD of ZrO_2 for low-temperature, large-area applications. ECS Journal of Solid State Science and Technology. 2017;**6**:N243-N249

[94] Gregory G, Wilson M, Ali H, Davis KO. Thermally Stable Molybdenum Oxide Hole-Selective Contacts Deposited using Spatial Atomic Layer Deposition. 2018 IEEE 7th World Conference Photovolt. Energy Convers. (WCPEC)(A Jt. Conf. 45th IEEE PVSC, 28th PVSEC 34th EU PVSEC) (pp. 2006-2009). IEEE. 2006-2009 (2018). DOI: 10.1109/PVSC.2018.8547343

IntechOpen